

UNDERSTANDING THE INFLUENCE OF TELLURIUM OXIDE IN THE FRONT
SILVER PASTE ON THE HOMOGENOUS HIGH SHEET EMITTER

by

Naga Sai Nirupama Bezawada

A thesis submitted to the faculty of
The University of North Carolina at Charlotte
in partial fulfillment of the requirements
for the degree of Master of Science in
Electrical Engineering

Charlotte

2016

Approved by:

Dr. Aba Ebong

Dr. Ed Stokes

Dr. Yong Zhang

©2016
Naga Sai Nirupama Bezawada
ALL RIGHTS RESERVED

ABSTRACT

NAGA SAI NIRUPAMA BEZAWADA Understanding the influence of tellurium oxide in front Ag paste for contacting silicon solar cells with homogeneous high sheet resistance emitter (Under the direction of DR. ABASIFREKE EBONG)

To reduce the cost of solar electricity requires highly efficient solar cells. However, the manufacturing of high efficiency solar cells does not match up with the cost. The higher the efficiency, the higher the cost. Thus, the high throughput technology such as screen printing, which dominates the manufacturing of solar cell needs to be reinvented to accommodate high efficiency at the same cost. This requires the use of transparent emitters for high short circuit current, open circuit voltage, and fill factor, which multiply to give the efficiency. Fill factor is often a problem with such lowly doped emitters, thus, a compatible front Ag paste must be formulated. This thesis, therefore, investigate such front Ag paste containing TeO_2 as compared to other pastes. It was found out that both the contact and gridline resistances for the TeO_2 containing paste are lower than the commercial counterpart paste. This is because, the TeO_2 functions as a catalyst, which decreases the viscosity of the molten glass during contact firing, leading to uniform etching of the underlying antireflection coating. Thus, large contact is formed, as well as highly conductive gridlines. The concentration of TeO_2 was found to be below the detection limit of EDS, as there was no trace of Te or its oxide after contact firing.

DEDICATION

This work is dedicated to *my dad Hanumantha Rao and mom Padma*

ACKNOWLEDGEMENTS

First, I thank God, the most merciful and compassionate, for allowing me to complete this thesis.

I would first like to thank Dr. Abasifreke Ebong, the principal investigator of this study and academic advisor. The door of Dr.Ebong's office was always open whenever I ran into a trouble spot or had a question about my research or writing. He consistently allowed this paper to be my own work, but steered me in the right the direction whenever he thought I needed it.

In addition I would like to thank Dr. Ed Stokes and Dr. Yong Zhang for taking time to serve on my thesis committee and guiding me in improvement of undertaking of the scientific research.

I would also like to thank my friends and family for their support and comprise that has allowed me to achieve my goals.

TABLE OF CONTENTS

CHAPTER 1: PHOTOVOLTAICS	2
1.1 Introduction	2
1.2 Basic Working of a Solar Cell.....	2
1.3 Electrical Output Parameters of a Solar Cell	3
1.3.1 Short Circuit Current (I_{sc})	3
1.3.2 Open Circuit Voltage (V_{oc})	4
1.3.3 Fill Factor (FF).....	5
1.3.4 Efficiency (η)	6
1.4 Current Transport Mechanism in Solar Cell	7
1.5 Motivation	8
1.6 Scope of the Work.....	9
CHAPTER 2: DESIGN OF HIGH SHEET RESISTANCE EMITTERS	10
2.1 Factors Affecting the Efficiency of a Solar Cell.....	10
2.1.1 Optical Losses.....	11
2.1.2: Electrical Losses	12
2.1.3 Impact of Resistance on solar cell efficiency.....	16
2.1.4 Ideality Factor:	19
2.2 Homogeneous High Sheet Resistance Emitter (HHSE) in Brief	19
CHAPTER 3: FRONT SILVER PASTE FORMULATION	21
3.1 Front Silver Paste Composition.....	21

3.2 Factors to be Considered When Formulating a Front Ag Paste:.....	24
3.3: Impact of Additives on Contact Formation.....	25
3.4 Screen Printing Technology	25
3.5 Contact Formation Mechanism:	27
CHAPTER 4: EXPERIMENTAL.....	30
4.1: Solar Cell Results.....	30
4.2 Specific Contact Resistance Measurements using Transfer Length Method.....	31
4.2.1 Sample Preparation:	32
4.3 Scanning Electron Microscopy:	35
4.4 Energy Dispersive Spectrometry (EDS)	38
4.5 Conclusion.....	41
REFERENCES	42

CHAPTER 1: PHOTOVOLTAICS

1.1 Introduction

A solar cell is a device which converts sunlight into electricity without any polluting byproduct. A solar cell consists of two dissimilar semiconductor layers, n and p, and in between these two layers there exists an electric field in the depletion region that enables the separation of the electron-hole pairs created in the quasi-neutral p-region immediately after the depletion region. The figure of merit of a solar cell is the efficiency, which can be influenced by the reflection of the incident light, absorption and generation of electron-hole pairs, separation and collection of carriers. It is the product of the open circuit voltage (V_{oc}), short circuit current (I_{sc}) and fill factor (FF). Each of these electrical output parameters have dependence on the bulk material quality, the p-n junction and the peak surface concentration of the emitter. FF in particular, which is what this thesis is investigating in relation to front silver paste, is impacted by the total series resistance made up of six components: namely; (i) gridline, (ii) emitter, (iii) contact, (iv) busbar, (v) bulk and (vi) back. For the screen-printed technology, which is adopted commercially because of its low-cost and high throughput, the fill factor is a function of the front Ag paste constituents.

The front Ag paste consist of three major components; namely, (a) Ag powder, (b) glass frit and (c) organic binders or vehicle. In addition, there are some additives such as

Zirconia , germanium, silicon and tellurium and/or tellurium oxide. The additives are used to tailor the paste to suit a purpose, especially overcoming the challenge of contacting transparent emitter. In this study, the influence of such additive, tellurium oxide (TeO_2), is investigated.

1.2 Basic Working of a Solar Cell

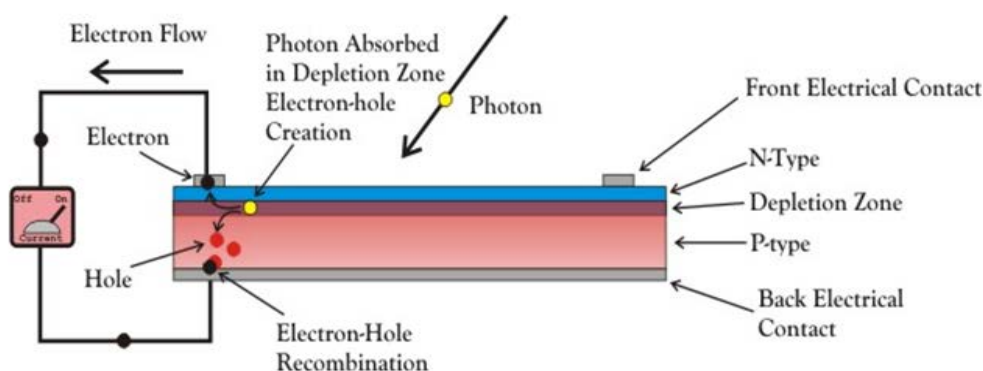


Figure 1.1: Working principle of solar cell

Figure 1.1 shows a typical working solar cell with p-type base having negative and positive electrodes on the top and bottom, respectively. When light of certain wavelength falls on the cell then the photons whose energy is equal to the band gap are absorbed. Then electrons move to higher energy states where they can move freely. These excited electrons create holes in the valence band. Due to the built in electric field in the depletion region, the charge carriers are attracted to the respective electrodes and current flows through external circuit. The absorption of light is effected by front surface texturing and antireflection coating (ARC) thickness and refractive index. The ARC helps in the better absorption of the light as well as decrease in front surface recombination, thus increase the efficiency of the cell.

1.3 Electrical Output Parameters of a Solar Cell

Fig. 1.2 shows the I - V output characteristics of an illuminated solar cell; i) open circuit voltage (V_{oc}), the voltage between two terminals when no current flows, ii-) short circuit current (I_{sc}), the current when the terminals are connected to each other, iii-) fill factor (FF), the ratio of the maximum obtainable power to the product of V_{oc} and I_{sc} .

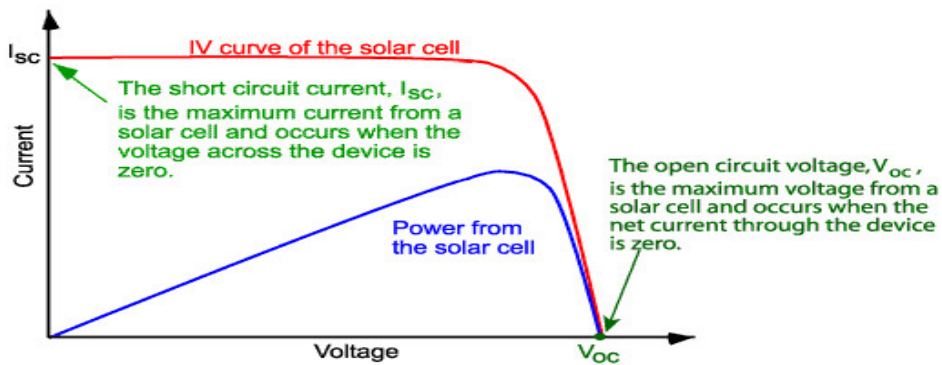


Figure 1.2: I - V Characteristic Curve [1]

1.3.1 Short Circuit Current (I_{sc})

I_{sc} depends on (a) the area of the solar cell exposed to sunlight, (b) number of incident photons, (c) the spectrum of incident light and (d) the collection probability.

$$I_{sc} = I_L - I_o \left(e^{\frac{qV}{kT}} - 1 \right) \quad (1)$$

Where I_L is light induced current, I_o is saturation current, q is electron charge, V is the voltage between the terminals, k is Boltzmann constant and T is temperature.

The below equation (2) incorporates the effect of series resistance and junction diffusion and recombination.

$$I = I_{SC} - I_{01} \left(e^{\frac{q(V_{OC} - IR_S)}{n_1 k T}} - 1 \right) - I_{02} \left(e^{\frac{q(V_{OC} - IR_S)}{n_2 k T}} - 1 \right) \quad (2)$$

n is the ideality factor, I_{01} is dark saturation current of the emitter I_{02} is reverse saturation current of the junction.

1.3.2 Open Circuit Voltage (V_{OC})

V_{OC} is the amount of forward bias on the solar cell due to the bias of the solar cell junction with the light-generated current. Equation (3) shows the dependence of V_{OC} is found by setting the net current equal to zero;

$$V_{OC} = \frac{nkT}{q} \ln \left(\frac{I_{SC}}{I_0} + 1 \right) \quad (3)$$

Where n is ideality factor, k is Boltzmann constant, q is carrier charge, T is temperature, I_0 is dark saturation current and I_{SC} is short circuit current.

The dark saturation current (I_0) depends on the number of minority carriers, which is due to injection, at the space charge region edge, and the diffusion length of minority (L_{eff}) carriers, as shown in Equation (4).

$$I_0 = \frac{qD_n n_i^2}{N_A} \times \frac{1}{L_{eff}} \quad (4)$$

where D_n is the diffusion constant, n_i is the intrinsic carrier concentration, N_A is doping level.

The dark saturation current is the sum of saturation current of the emitter and the base or;

$$I_o = I_{oe} + I_{ob} \quad (5)$$

1.3.3 Fill Factor (FF)

FF is a measure of squareness of an I - V curve. FF is directly affected by the values of the cell's series and shunt resistances, ideality factor (n) and reverse saturation current (I_{o2}). Increasing the shunt resistance and decreasing the series resistance (R_s) will give higher FF . Thus, resulting in higher efficiency and bringing the cell's output power closer to its theoretical maximum [2], FF can be expressed as the ratio of the maximum power to the total power of a solar cell;

$$FF = \frac{I_m \times V_m}{I_{sc} \times V_{oc}} \quad (6)$$

where, I_m is the maximum obtainable current, V_m is the maximum obtainable voltage.

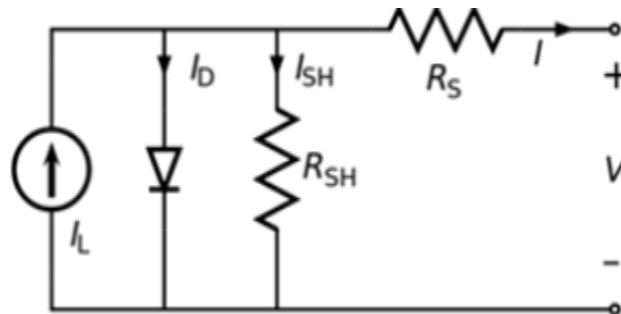


Figure 1.3: Equivalent circuit of a solar cell

Figure 1.3 represents the equivalent circuit of a solar cell showing series and shunt resistances.

Figure 1.4 depicts the six components of the series resistance of a solar cell as mentioned earlier, which are (i) R_{busbar} , busbar (ii) R_{back} , back (iii) $R_{emitter}$, emitter (iv) $R_{contact}$, semiconductor/gridline (v) $R_{gridline}$, gridline and (vi) R_{bulk} bulk

semiconductor. The total series resistance can be expressed mathematically in equation (7) [3].

$$R_s = R_{busbar} + R_{back} + R_{emitter} + R_{contact} + R_{gridline} + R_{bulk} \quad (7)$$

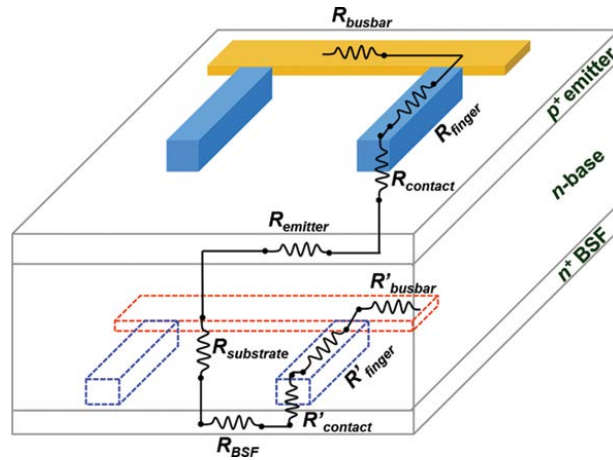


Figure1. 4: Breakdown circuit of the series resistance of a solar cell

$R_{emitter}$, R_{finger} and $R_{contact}$ dominate the total series resistance of a solar cell and impact the FF . Therefore, understanding of the contact and gridline sintering is critical to reducing the total series resistance to $<0.5\Omega/\text{cm}^2$ that is required to have less impact on FF .

1.3.4 Efficiency (η)

The efficiency (η) is the ratio of the electrical output of a solar cell to incident energy in the form of sunlight. The parameters V_{oc} , I_{sc} , and FF , must be optimized to increase the efficiency (η) of a solar cell given by Equation (8)

$$\eta = \frac{I_{sc} \times V_{oc} \times FF}{P_s} \quad (8)$$

where P_s is the power density of incident light

The efficiency of a solar cell has been the main challenge to overcome because it plays a deterministic role in the cost of solar electricity. The higher the efficiency obtained from a solar cell, the lower the cost per unit product. There has been always a trade-off between efficiency and cost in the industry to enable cost reduction.

1.4 Current Transport Mechanism in Solar Cell

The design of a high efficiency solar cell requires high absorption of photons, generation and separation of electron hole pairs near the junction in the quasi neutral region, and collection of these charges in the respective contacts. The carriers after separation by the inbuilt electric field must travel to the respective majority carrier regions to be collected by the metal contacts. Depending on the emitter peak surface carrier concentration, the potential barrier can be high, moderate or low. Each of which condition leads to one of the three types of current transport mechanisms: (i) thermionic, (ii) field, and (iii) thermionic field emissions.

Doping concentration dictates the current transportation process in a solar cell. The doping concentration in metal-semiconductor contact affects the width of the depletion region leading to the effect on Schottky barrier height. When the doping concentration is low ($< 10^{17} \text{cm}^{-3}$), the depletion region is wide. The electrons overcome the barrier height by possessing higher energy than the barrier height – the thermionic emission transport mechanism (Figure 1.5a). When the doping concentration is moderate ($< 10^{18} \text{cm}^{-3}$), thin barrier of 2-3nm is formed, then the electrons see moderate barrier height which they can tunnel through as well as going over with moderate energy – the thermionic field emission transport mechanism (Figure 1.5b). When the emitter is doped to a high concentration

($\sim 10^{20} \text{ cm}^{-3}$), then the barrier height is low and electron can tunnel through - the field emission transport mechanism (Figure 1.5c).

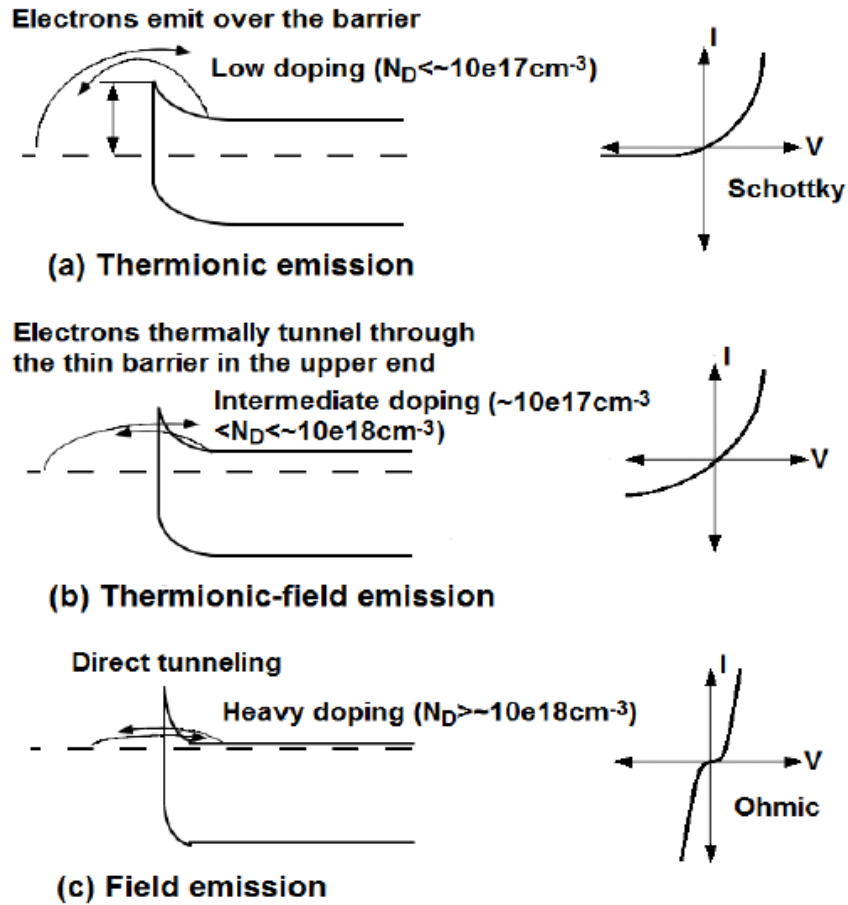


Figure 1.5: Current transport mechanism in a solar cell [4]

1.5 Motivation

The aim of the screen-printed technology is to capitalize on the cost effectiveness and high throughput to produce high efficiency without any additional cost. Therefore, to achieve this goal, the design of a solar cell must include transparent emitter, which does not necessarily favor the screen-printed technology. It is generally known that, the higher the transparency of the emitter, the more challenging it is to contact the emitter with high

FF [5]. This is due mainly to high contact resistance, which dominates the total series resistance. To overcome the high contact resistance on transparent emitter, front Ag pastes with a host of additives including TeO_2 , have been explored. Forming high sheet resistance emitter normally leads to non-uniformity in the emitter peak surface concentration and hence non-uniform contact formation [3]. To circumvent the non-uniform contacts, despite the variance in emitter sheet resistance, a front Ag paste which can contact a wide range of emitter peak surface concentration and achieve high FF should be investigated. In this study a TeO_2 containing paste is investigated in relation to forming a low contact resistance on transparent emitter.

1.6 Scope of the Work

Since screen printing technology is inexpensive, simple and high throughput, most solar cell manufacturers adopt this technology. However, because of the fire through dielectric of the metal contacts, formation of ohmic contact on high sheet resistance emitter is challenging [6]. In this work, high sheet resistance emitter was contacted with two pastes (i) TeO_2 containing and (b) no TeO_2 containing counterpart. The cells were evaluated based on FF and R_s (mainly contact resistance component based on TLM measurements), SEM analysis was carried to understand the microstructures in each paste and EDX to trace the elements present after contact formation.

CHAPTER 2: DESIGN OF HIGH SHEET RESISTANCE EMITTERS

2.1 Factors Affecting the Efficiency of a Solar Cell

Depending on the energy bandgap of a semiconductor, Si for example, the open circuit voltage should be $\sim 1.1\text{V}$. However, this is not practically attainable because a large part of the energy from the sun irradiation incident on a solar cell is wasted instead of being converted into electrical power. There are several factors responsible for these losses including the quality of the bulk material, reflectance from the surfaces, and how the solar cell is designed. These losses can be categorized in two groups (i) optical and (ii) electrical as summarized in Figure 2.1.

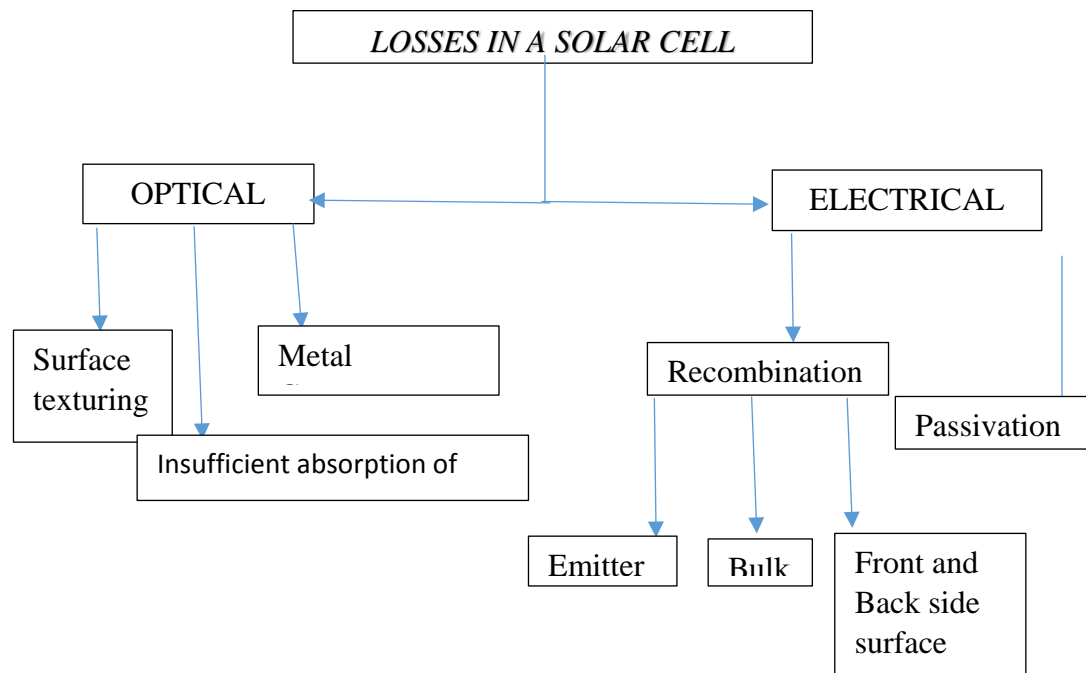


Figure 2.1: Factors affecting the efficiency of a cell

2.1.1 Optical Losses

The optical losses in a solar cell include (i) reflectance, (ii) shadowing and (iii) insufficient absorption. This is summarized in Figure 2.2.

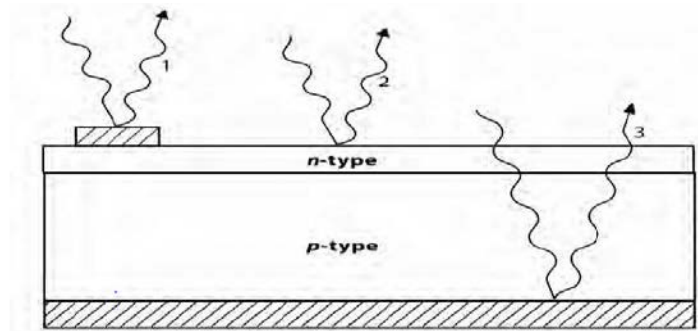


Figure 2.2: Optical losses on a cell, (1) surface reflection (front and back) (2) front contact shadowing and (3) insufficient absorption [7]

2.1.1.1 Reflectance

Figure 2.2 shows the light reflection from three parts of the cell, the front metal contact, the front and back surfaces of the cell. To achieve high efficiency will require decreasing the front surface reflectance. This can be decreased by surface texturing, which involves the use of potassium hydroxide in the presence of isopropanol alcohol at 80-90°C for 20-25 mins. Surface texturing decreases the surface reflectance from ~30% to ~12%. This action produces random pyramids at the surface of silicon with heights of ~2-4 μm . Further reduction in reflectance is effected by adding antireflection layer (ARC) such as SiN_x (~73 nm and index of refraction of ~2.03). A combination of surface texturing and ARC reduce the reflectance to ~4%. Thus, without ARC, the silicon would only transmit about 70% of IR and 50% of UV portions of the sunlight into the cell [8].

The reflection coefficient can be reduced by covering the top of the solar cell surface by antireflective coatings (ARC). The surface of the silicon substrate can be covered with single or double antireflective coatings. To achieve lowest reflection of a single wavelength of incident radiation, the ARC must retain (a) square root of the refractive indices of the materials constrained the coating equal to the refractive index of the ARC and (b) thickness of ARC equal to one quarter of the wavelength [9]. The proper choice of thickness of the ARC is important for the metallization process of electrical contacts. Excessively thick ARC makes the process of contact fire through dielectric more difficult, and additionally decreases optical parameters and efficiency of the solar cell.

2.1.1.2: Shadowing

The gridline and busbars on commercial silicon solar cell can contribute ~8% shadowing on the front surface, which further reduces the number of photons that could be absorbed. This is the area which attracts ongoing research to keep the gridlines as narrow as possible (<40 μm).

2.1.1.3 Insufficient Absorption of the Light

Also, photon energy larger than the bandgap of the bulk material can escape from the backside and not absorbed. Equally true for photons with energy lower than the bandgap to be converted to heat at short wavelength and thus no absorption.

2.1.2: Electrical Losses

An electron exists in the metastable state in the conduction band and it moves to the valence band emitting energy in the form of heat or light. When it moves to the valence band it combines with the hole. This is called recombination. Recombination losses affect

the current collection and the forward bias injection current. Thus recombination current affects the open circuit voltage and short circuit current. Factors impacting the efficiency of a solar cell from the electrical perspective include the following (i) emitter, (ii) front and back surface, (iii) bulk and (iv) contact recombination.

2.1.2.1 Bulk Recombination:

There are three types of bulk recombination, namely: (i) Radiative, (ii) Shockley, Read Hall (iii) and Auger.

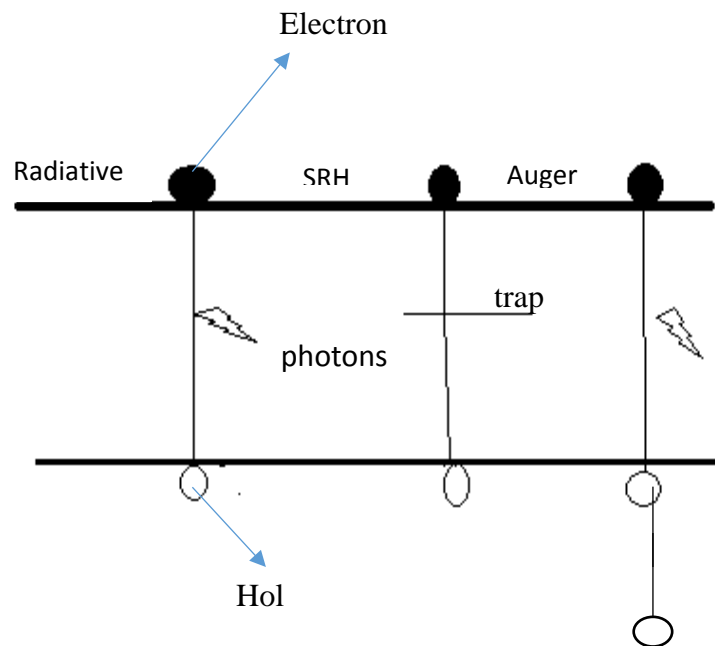


Figure 2.3: Types of Bulk recombination

$$\frac{1}{\tau_{bulk}} = \frac{1}{\tau_{radiative}} + \frac{1}{\tau_{Auger}} + \frac{1}{\tau_{SRH}} \quad (9)$$

Recombination depends on the minority carrier lifetime and diffusion length. It is the average time which a carrier can spend in an excited state after electron-hole generation before it recombines. Diffusion length is the average length a carrier moves between

generation and recombination. Semiconductor materials that are heavily doped have greater recombination rates and consequently, have shorter diffusion lengths. Higher diffusion lengths are indicative of materials with longer lifetimes, and is therefore an important quality to consider with semiconductor materials.

Bulk lifetime, dependent on dopant and excess carrier concentrations, was modeled by modifying the semi-empirical expression [10]:

$$\frac{1}{\tau_b} = \frac{1}{\tau_{bo}} + N_D (1.8 \times 10^{-24} N_D^{-0.65} + 6 \times 10^{-25} \left(\frac{n_i}{N_D} \right)^{0.65} + 3 \times 10^{-27} \times \Delta n^{0.8}) \quad (10)$$

Δn is the excess carrier concentration, N_D is base material doping, n_i is intrinsic carrier.

The value of bulk doping level will control minority carrier lifetime [12]. τ_{bulk} will decrease as the value of doping concentration increases. The above equation accounts for both the Auger recombination which dominates over SRH and radiative recombination. Acceptor doping concentration, N_A will affect minority carrier lifetime. An increase on N_A will reduce minority carrier lifetime. Direct effect of reduction on minority carrier lifetime is a decrease on short circuit current I_{SC} . The increase of V_{oc} is done through the reduction of the photo generated current (I_0) which is done via increase of N_A and N_D

2.1.2.2 Front and Back Surface Recombination:

The surface of the solar cell represents a severe disruption of the crystal lattice, the surfaces of the solar cell are a site of particularly high recombination. The defects at a semiconductor surface are caused by the interruption to the periodicity of the crystal lattice, which causes dangling bonds at the semiconductor surface. The reduction of these defects

is done by passivating the layer. The back side of the cell is alloyed with Al metal which forms the back-surface field (BSF) and provides a high potential to reflect the minority carriers to the front side to be collected. Thus the BSF provides a mirror for the minority carriers without which they will recombine at the back surface and reduce the VOC and hence the efficiency of the cell.

2.1.2.3 Contact Recombination:

Contact recombination can be reduced by introducing dopant underneath the metal contacts such as the case with selective emitter. The heavy doping under the front and the back contacts helps the cell from high recombination at the contacts (Figure 2.4). This helps to increase the efficiency of the solar cell because J_{02} is low. However, for screen printed cells without the contact diffusion, the paste should be flexible enough to result in low contact recombination.

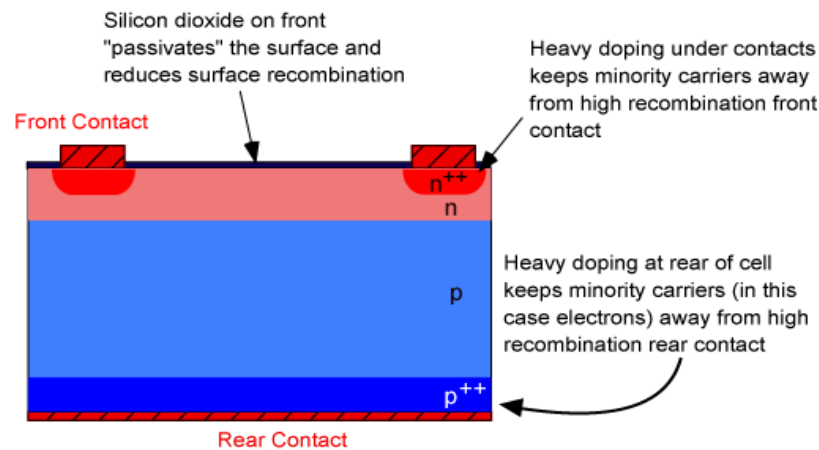


Figure 2.4: Influence of doping of contacts and passivation on the recombination

2.1.2.4 Emitter Recombination (J_{0E}):

The main function of the emitter is the collection of light-generated minority carriers. If a high level of phosphorus is diffused into silicon, the excess phosphorus lies at

the surface of the cell, creating a 'dead layer', where light-generated carriers have little chance of being collected [7]. Besides this feature, lowly doped emitters have also a passivation effect by suppressing the recombination at the semiconductor surface. The cell efficiency and short-circuit current decrease with increases in emitter doping. Thin emitters offer higher cell performance because of reduced recombination. Lightly doped emitters offer better cell performance due to increased minority carrier diffusion lengths. In a high sheet emitter, the excess dopant higher than $3\sim 5\times 10^{20}/\text{cm}^3$ is electrically inactive and creates Shockley-Read-Hall (*SRH*) recombination centers in the layer. Such recombination sources generate thermal minority carriers and increase the dark saturation current of the solar cell device, resulting in lower V_{oc} [11].

2.1.2.5 Junction Recombination (J_{02}):

As recombination life-time of the charge carriers is inversely proportional to the trap density, hence the presence of higher trap density reflects the lower recombination life-time of charge carriers as well as higher recombination losses [13]. Annealing reduces the trap density and hence improves the life-time of charge carriers, which reduces the recombination losses in the device. So, the value of J_{02} is lower if the cell is annealed. At low voltage, J_{01} (diffusion saturation current) is lower than J_{02} and reverse trend in high voltage region.

2.1.3 Impact of Resistance on solar cell efficiency

The efficiency of a solar cell depends on the FF , V_{OC} and I_{SC} . The FF and I_{SC} are affected by the series resistance while V_{OC} is not because there is no current flow during its measurement as the name suggests. However, since efficiency is the product of the three

parameters, series resistance invariably impact all the parameters. Shunt resistance (R_{SH}) on the other hand influence V_{OC} as well as FF but not I_{SC} . The lower the value of R_{SH} , the poorer the V_{OC} and FF but I_{SC} stays the same.

2.1.3.1 Series Resistance:

Series resistance in a solar cell has three causes: firstly, the movement of current through the emitter and base of the solar cell; secondly, the contact resistance between the metal contact and the silicon; and finally, the resistance of the top and rear metal contacts. The major contributors to the series resistance (R_s) are the bulk resistance of the semiconductor material, the metallic contacts and interconnections, carrier transport through the top diffused layer, and contact resistance between the metallic contacts and the semiconductor. The main impact of series resistance is to reduce the fill factor, although excessively high values may also reduce the short-circuit current. The series resistance made up of six components, base, contact, emitter, gridline and the bus-bar resistance [14]. Figure 2.5 shows the impact of series resistance on the I-V curve of a solar cell. The V_{OC} is seen to be unaffected by the series resistance because in the three values demonstrated, the V_{OC} stays the same while the I_{SC} decreases when the series was very large.

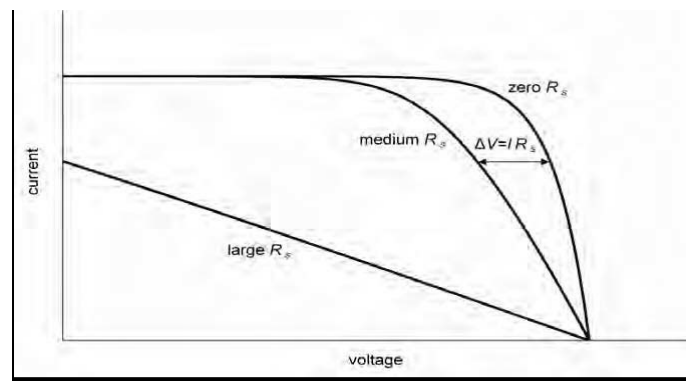


Figure 2.5: Effect of series resistance on the I-V characteristics of a solar cell

2.1.3.1.1 Effect of Series Resistance on the FF and Efficiency of the Cell:

While attempting to improve the performance of the cell, we need to focus on the emitter and contact resistance of the cell. Contacting emitters with a low total phosphorous concentration (i.e. $R_{sheet} > 80 \Omega/\text{sq}$) with screen-printed technology, leads to very high contact resistances [15]. With an increase in the contact resistance there is an increase in the overall series resistance which in turn led to lower FF . The reduction in FF corresponding to the total series resistance is given by [16]:

$$DFF = -\frac{J_{sc}}{V_{oc}} \times R_s \times FF \quad (11)$$

The high-quality contacts on the cell lead to the reduction of junction recombination and series resistance and an increase in FF [17].

2.1.3.3 Shunt Resistance:

A low shunt resistance results in the low solar cell efficiency. If the shunt resistance is low the open circuit voltage of the cell is also low. The shunt resistance is caused by improper diffusion of Ag particles into the junction during contact firing and any metal contact shorting the p-n junction. An estimate for the value of the shunt resistance of a solar cell can be determined from the slope of the I - V curve near the short-circuit current point. Figure 2.6 shows the impact of shunt resistance on the open circuit voltage of a solar cell. The smaller the shunt resistance, the higher the impact on the open circuit voltage. Thus, for a high efficiency solar cell, the shunt resistance value should be very high, so that at maximum power, when there is current flow, as shown in the equivalent circuit of a solar cell, there is no current flow through the junction and the terminal voltage will be high.

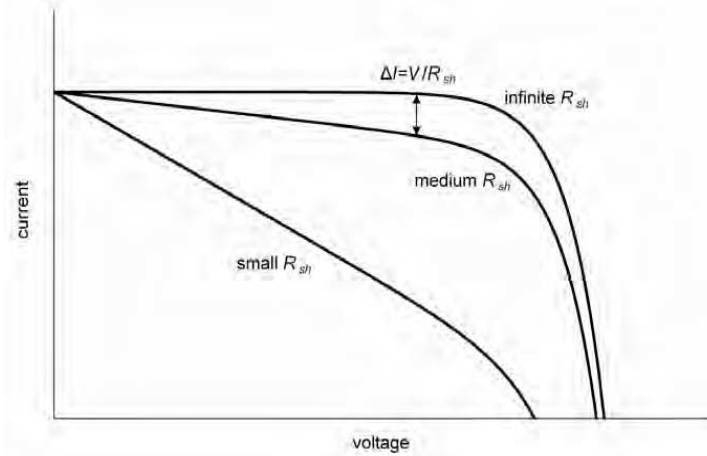


Figure 2.6: Effect of shunt resistance on the I-V characteristics of a solar cell

2.1.4 Ideality Factor:

The ideality factor of a diode is a measure of how closely the diode follows the ideal diode equation. Thus, if the ideality is higher than 1.05, the impact will be exhibited in the FF. For a highly efficient solar cell with excellent contact, the ideality factor is close to 1.05. The deviation of an ideality factor from unity reduces the solar cell efficiency [13].

2.2 Homogeneous High Sheet Resistance Emitter (HHSE) in Brief

Key to increasing the efficiency of a solar cell is the design of the emitter to decrease the electrical losses (emitter dark saturation current density – J_{OE}) in addition to reducing the optical losses. The peak surface concentration of dopant at the emitter and junction depth are critical to obtaining high V_{OC} and I_{SC} . If the emitter is optically transparent (lightly doped or low peak surface concentration), J_{OE} will be low, thus, high I_{SC} and V_{OC} would be attained. However, transparent emitter is difficult to contact, especially when using the screen-printing technology. Partly because of the high non-uniformity in such emitter, which results in varying peak surface concentrations and junction depths of the emitter. Thus, the presence of high series resistance points due to

high contact resistance in the area with low peak surface concentration [18]. High series resistance certainly degrades the FF [19] of a solar cell. For example, Figure 2.7 shows the breakdown of the series resistance components of a typical commercial silicon solar cell with varying sheet resistance emitter. It is seen that the contact resistance increases as the emitter sheet resistance with fixed number of gridlines (74).

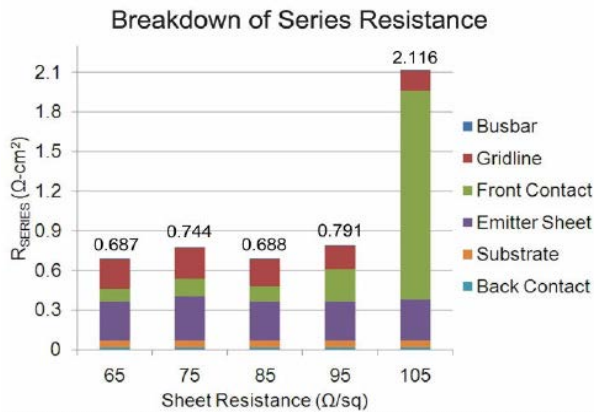


Figure 2.7: Contribution of the emitter resistance in overall series resistance in HHSE [19]

Thus, contact resistance must be reduced to improve the efficiency of a screen-printed solar cell, which requires high sheet resistance emitter. The solution therefore, lies in the front Ag paste in addition to sintering to achieve low contact resistance on high sheet resistance emitters. That is where the TeO_2 containing paste becomes handy in this investigation

CHAPTER 3: FRONT SILVER PASTE FORMULATION

3.1 Front Silver Paste Composition

The front silver paste composition and peak firing temperature influence the contact quality of a solar cell. The paste contains metal powder, glass frit and organic medium (resin), and some additives as shown in Figure 3.1. The Ag powder particle size and morphology controls the gridline and contact resistance. The glass frit morphology, size and transition temperature influence the sintering of the gridlines and contact quality. The amount of glass frit determines how fast the underlying ARC layer is etched. The amount of Ag loading determines the viscosity of the paste. While the organics control the rheology of the paste, which in turn affect printing

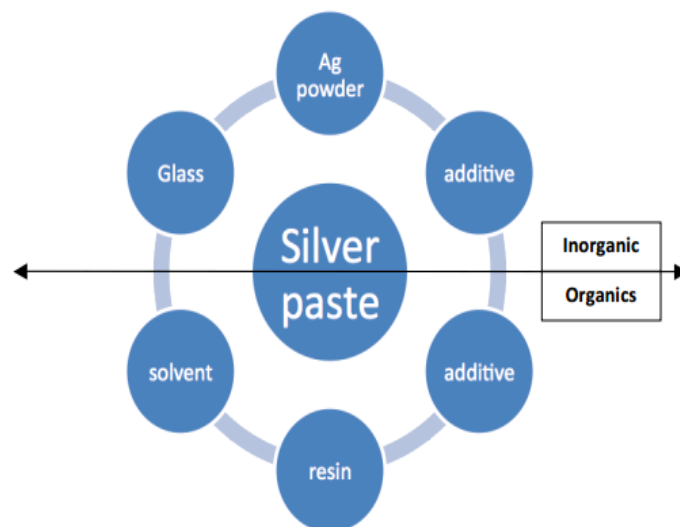


Figure 3.1: Pictorial representation of the components present in the front Ag paste

Some of the glass frits found in front Ag paste include the oxides like PbO, ZnO, Al₂O₃, SiO₂, TiO₂, MnO etc. About 5% of the paste is the glass frit. This helps in etching of the ARC layer during contact and gridline sintering as mentioned earlier. The reactive molten glass frit etches and forms a thin silicon layer at the interface. The etching process depends on glass frit composition, percentage of the glass frit, crystal orientation and peak firing temperature. These are important to form a stable and conductive contact between the Ag and Si interface. Etching process produces recrystallized glass at the interface of Si and ARC leading to the formation of MOS (metal- oxide- semiconductor) contact, see Figure 3.2. This formation of contact reduces the potential barrier height between the metal and Si if the oxide is thin ~10 nm. Thus, electrons can tunnel through the oxide and be collected. This mode of conduction results in a cell with high FF [21]. However, if the oxide is >10 nm, this will result in high barrier height and electrons must overcome the barrier to be collected as in thermionic emission.

The glass frit transition temperature and the softening characteristics affect the interface structures. The transition temperature also affects the contact ohmicity of the thick film metal grid. High transition temperature results in forming a thinner glass region between the Ag bulk and Si emitter. Sintering temperature is the temperature at which the material forms a solid mass without melting. The cell which has a glass frit with higher transition temperature crystallizes fast during the firing cycle after the ARC etching and Si emitter formation results in low density of Ag crystallite precipitate. This results in low J_{02} and higher V_{oc} [22].

Glass frit also helps in the adhesion of the gridline to the semiconductor substrate in addition to sintering kinetics of the metal powder. It is a mixture of metal oxides and

silicon dioxide melted to form a uniform glass. Before is added to the paste, the glass is milled to a thin sheet and crushed. During firing, the oxide is necessary as required for adhesion since molten glass frit is very effective in etching silicon oxide [23]. The glass frit in the Ag paste is the main factor that determines the contact resistance, silicon surface etching, and ultimately the overall surface performance. Formation of the metal contacts should result in the low contact resistance, good adhesion, good solderability high gridline conductivity and minimum silver penetration into silicon surface. The silver ink is affected by the percentage of the glass frit and the type of the glass frit, the size and shape of the silver grain.

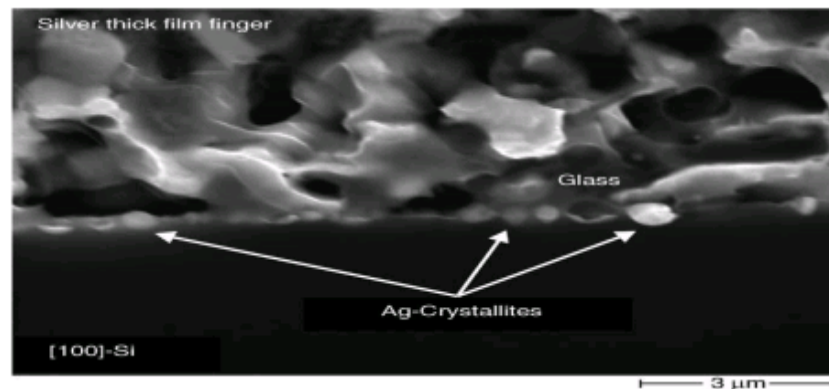


Figure 3.2: SEM- the interface between the Ag and Si [24]

The organics on the other hand act like carrier medium for the powder and glass frit to mix (Figure 3.3). During the sintering of the metal contacts, the organics burn off before the sample reaches the peak firing temperature. After drying the contact is formed at a temperature below the silver/silicon eutectic temperature of 836°C. The organics also control the viscosity and rheology of the paste.

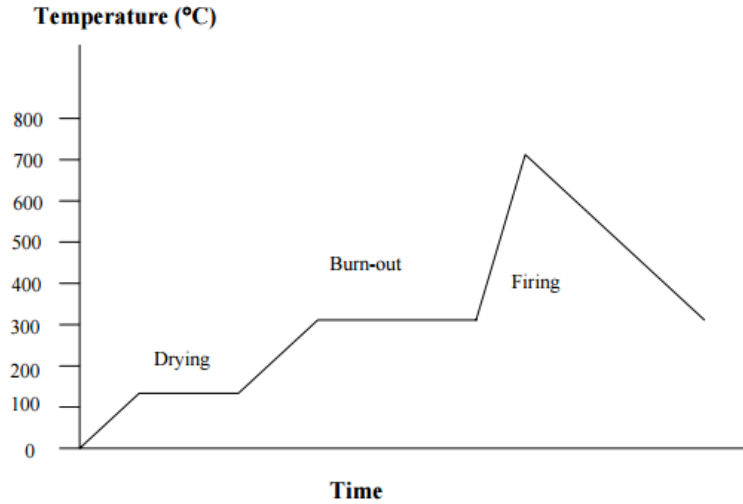


Figure 3.3: Schematic of temperature profile in belt furnace

Silver powder is used for its high conductivity and the work function closer to that of silicon. This lower barrier helps in cohesion with the contact and promotes electrical conductivity of the paste [25]. For a screen-printed cell, the paste has 85-90% of Ag powder. For a six-inch silicon, the amount of silver paste used is ~100 mg.

3.2 Factors to be Considered When Formulating a Front Ag Paste:

- Line conductivity
- Finger aspect ratio
- Adhesion strength
- Firing Window
- Low contact resistance irrespective of emitter sheet rho

Field emission is the most desired current transport mechanism because it indicates an ohmic contact formation which is associated with low contact resistance for high FF. Formation of ohmic contact requires a metal whose work function is close to that of the

semiconductor. However, for evaporated contacts and use of forming gas anneal, this can easily be achievable. But for the screen-printed technology where the metal fires through the dielectric and contact regions with wide variation of surface concentration, it is difficult. Thus, the paste formulation must consider the importance of the work function match between the metal and Si.

3.3: Impact of Additives on Contact Formation

Additives are added to tailor the front Ag paste to form low contact resistance on lightly doped emitter (or homogenous high sheet resistance emitter - HHSE). In 2006, Ebong et al [20] reported some improvement on cell performance as a result of additives to the base paste. However, the series resistance on lightly doped emitter was still higher than needed to achieve FF of >80%. In 2010 [19], another type additive was used which enabled the contacting of HHSE with improved performance. This paste can be linked to patent number US 8,497,420 B2, which incorporates tellurium oxide [30]. This paste consists 85-99.5% conductive metal, 0.5-15% of the lead-tellurium oxide in which mole ratio of lead to tellurium can be 5/95 or 95/5 and an organic medium. It has an electrical conductive metal, lead-tellurium oxide dispersed in organic medium. This formulation is not meant to etch the surface too deep, so a small amount of glass frit is present in the paste. This glass frit also helps in the transport of charge carriers in between Ag and recrystallized Si emitter.

3.4 Screen Printing Technology

The principle of screen printing is shown in Figure 3.4. A pattern is photographically defined on a stainless-steel screen by means of an emulsion layer. A paste

of the material to be screen printed is pressed through the screen by means of a squeegee.

Important screen printing parameters are:

- (i) the viscosity of the paste,
- (ii) the mesh number of the screen,
- (iii) the snap-off distance between the screen and the substrate
- (iv) the pressure and
- (v) speed of the squeegee.

After leveling, the printed wet film is dried (e.g. at 200 °C, 2 min) – Figure 3.4. By then, the film consists of loose conglomerates of very small grains (1- 2 μm). The sintering step results in a compact film, where large grains (e.g. up to 10 μm) are electronically and optically intimately connected.

Sintering is a high temperature step (typically 500 to 800 °C), and is usually performed in an oven with a transport belt. In many cases an inert nitrogen atmosphere in the oven is required. Often a “sinter flux” is added to the paste. At the sintering temperature, this flux is melting, and forms a liquid in intimate contact with the solid grains. Sintering is then enhanced by the mechanisms of liquid phase sintering because of the glass frit. At first, there is a rearrangement of the grains due to capillary forces; then, small grains are dissolving in the liquid flux, and material is condensed on the larger grains; next, in a coalescence phase, material is dissolved from places with positive curvature, and deposited at places with negative curvature; finally, neck growth can occur, when two grains are separated by a capillary liquid film. For all these mechanisms to happen, it is necessary that the liquid sinter flux completely wets the solid grains, and that the solubility of these

grains in the liquid flux is high enough. Finally, in the materials systems under discussion, the sinter flux should be volatilized completely at the end of the sintering process [26].

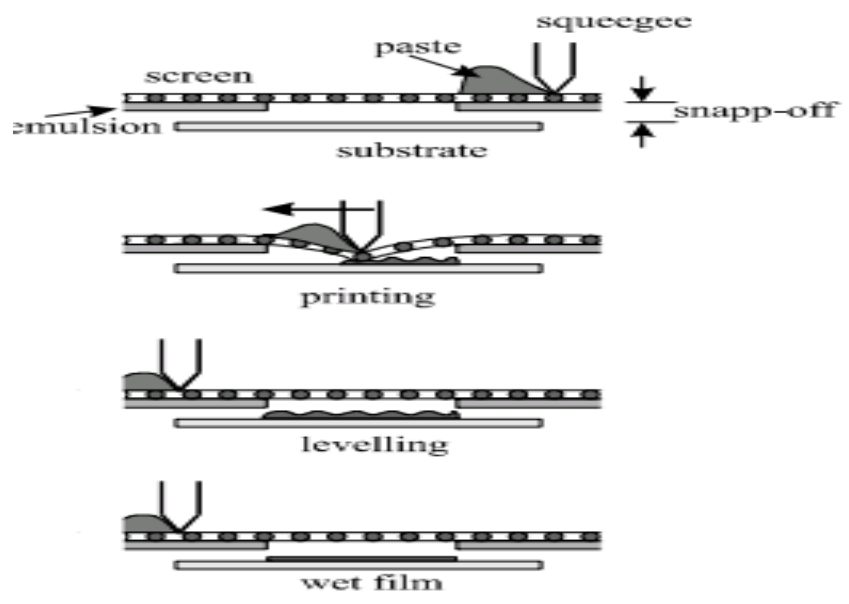
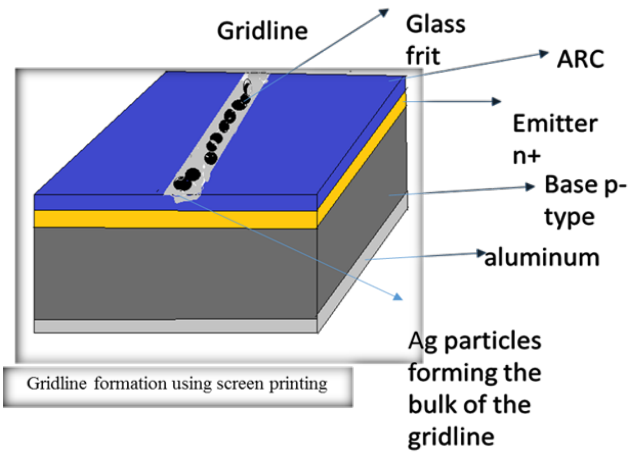
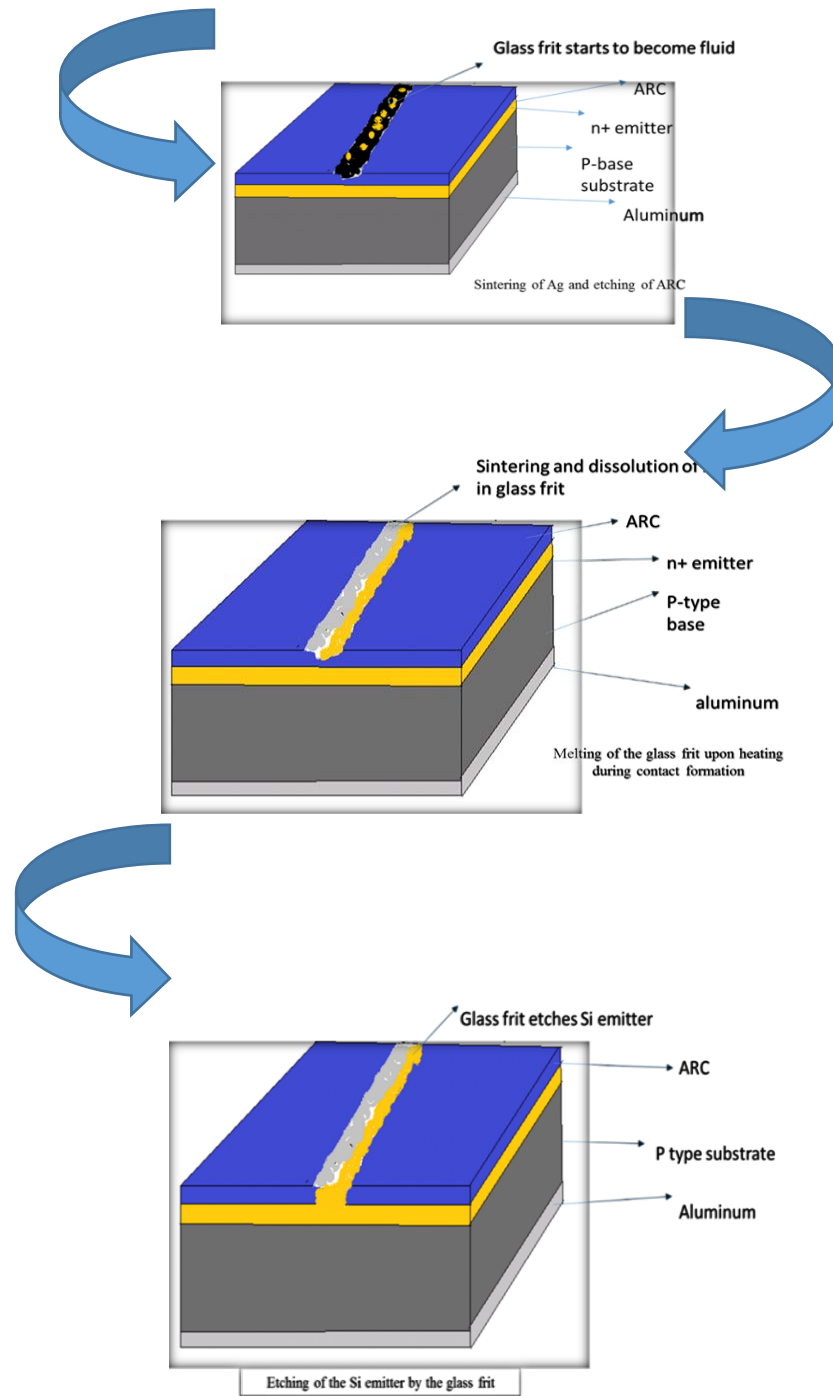


Figure 3.4: Screen printing technology [26]

3.5 Contact Formation Mechanism:

Pictorial representation of the contact formation on screen-printed silicon solar cell as shown in figure 3.5:





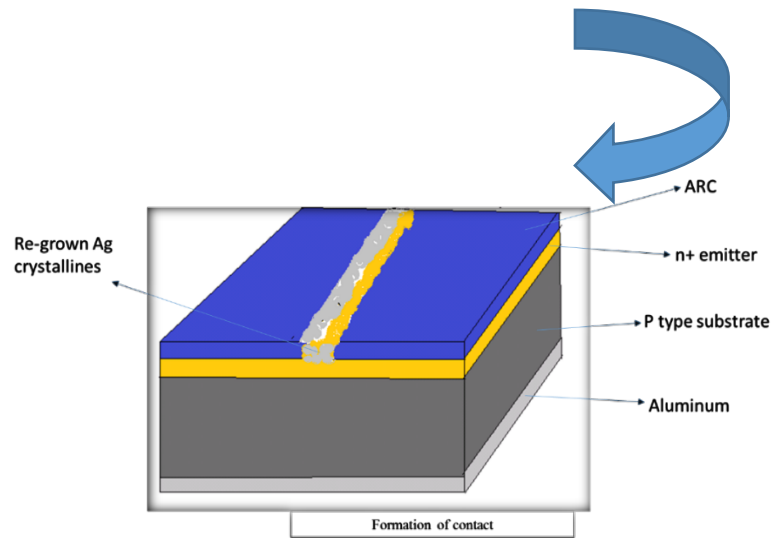


Figure 3.5: Contact formation process

The contacts are formed when screen-printed film is heated at a temperature above 750°C. Upon heating the glass frit fluidizes and wets the *ARC* surface, dissolving the silver and etches the *ARC* layer [27]. The redox reaction taken place in the etching of *ARC* layer is $\text{Si} + \text{MO}_x \rightarrow \text{SiO}_2 + \text{M}$ [28]. There are metal precipitates present at the metal and substrate interface. The glass frit etches small amount of silver and the metal is precipitated at the glass after firing [29]. On cooling excess Si crystallizes at the epitaxial on the substrate. The dissolved metal is alternatively oxidized and precipitate in the glass layer. The glass frit starts to melt at temperature of 450°C.

CHAPTER 4: EXPERIMENTAL

The screen-printed solar cells utilizing the two pastes; TeO₂ containing and the counterpart without was fabricated and the (i) efficiency (ii) FF (iii) specific contact resistance was measured based on TLM. This was followed by SEM and EDX after the wafers were cut into shape to fit into the SEM chamber.

4.1: Solar Cell Results

Table 4.1 lists the electrical output parameters of solar cells comparing three front contacts pastes. Note that the TeO₂ containing paste showed the best performance compared to both the commercial and non-TeO₂ containing pastes. In particular, the series resistance is lower for the TeO₂ containing paste than the other two. The average FF for this special formulation is higher than the other two. This indicates that both the contact and gridline resistances are lower than the two counterparts. All cells were fired at the same temperature without any optimization for peak firing temperature for any of the pastes.

Table 4.1: Electrical output parameters of the solar cells with high sheet resistance emitter for the TeO₂ and non-TeO₂ pastes compared to the commercial paste.

Sample ID	Voc (mV)	Jsc (mA/cm ²)	FF (%)	Efficiency (%)	Ideality Factor (n)	Rs (Ω-cm ²)	Pseudo FF (%)
TeO ₂ -5	638.1	37.3	78.7	18.7	1.035	0.7407	82.6
TeO ₂ -4	637.9	37.3	80.0	19.0	1.037	0.4691	82.4
TeO ₂ -3	638.2	37.3	79.3	18.9	1.031	0.6364	82.6
TeO ₂ -2	637.3	37.1	80.3	19.0	1.040	0.3060	81.9
TeO ₂ -1	638.1	37.4	79.4	19.0	1.032	0.6568	82.8
HP-5	634.8	37.6	79.4	18.9	1.040	0.6153	82.6
HP-4	637.1	37.4	78.1	18.6	1.035	0.8854	82.7
HP-3	637.7	37.7	78.7	18.9	1.025	0.9251	83.5
HP-2	636.8	37.7	78.3	18.8	1.031	0.9436	83.2
HP-1	637.6	37.7	79.1	19.0	1.033	0.8373	83.5
No TeO ₂ -5	635.8	37.1	68.0	16.0	1.014	2.9927	82.0
No TeO ₂ -4	635.7	37.2	68.8	16.3	0.996	2.8779	82.5
No TeO ₂ -3	635.3	37.3	67.1	15.9	0.992	3.3932	82.7
No TeO ₂ -2	635.6	37.2	70.2	16.6	1.003	2.4138	82.4
No TeO ₂ -1	636.3	37.2	68.8	16.3	0.992	2.8416	82.5

Specific contact resistance measurements was carried out using the transfer length method as outlined in the next section.

4.2 Specific Contact Resistance Measurements using Transfer Length Method (TLM):

The four-point probe method of measuring the contact resistance has been generally accepted. The TLM pattern that are of uneven contact spacing are normally used (Figure 4.1). However, the contact resistance is a strong function of the method of fabrication of the device. Light emitting diodes, transistors, sensors etc, use evaporated or sputtered bulk

metal for their fabrication, thus the contact resistance is different than the solar cell, which uses screen-printed or fire through dielectric contacts. For micro devices like the LED and transistors, the TLM [31] pattern works very well to give accurate values of the contact resistance. However, for solar cells, which are macro diodes, the same TLM pattern does not give a representative contact resistance because of some effects such as the emitter non-uniformity. That is why Meier et al [32] introduced a method of contact resistance measurement with the solar cell gridline pattern. In this work the Meier et al method is used, where the solar cell was cut in two millimeter strips with the gridlines perpendicular to the cut.

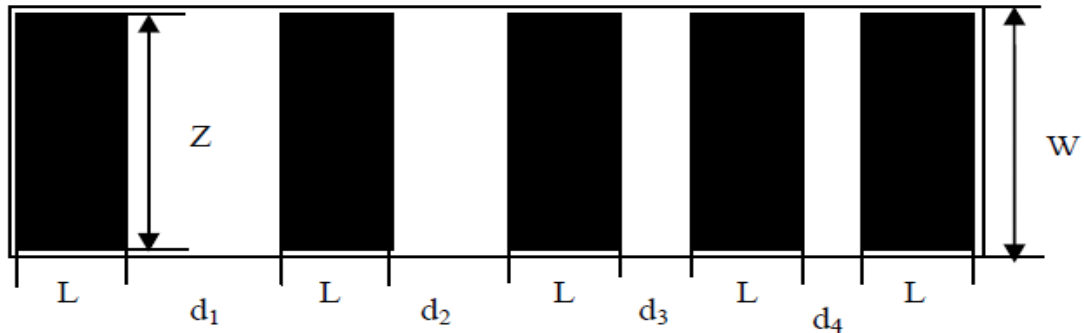


FIGURE 4.1: Transfer Length Method Test Structure

4.2.1 Sample Preparation:

In this study contact resistance measurement was carried out one cell each as per type of paste. The sample is cut into 2mm strips with gridlines perpendicular to the cut. The cut sample was placed under a USB High Zoom microscope and the software Dino-Capture 2.0 was utilized to capture the image and measure the gridline width (measured in micro-meters). After the finger width was measured and recorded, the formula: $\text{gridline-spacing} = 155/88 - \text{gridline-width}$ was used. The 155 represents the length of the solar cell

in millimeters and the 88 represents number of spaces between the fingers (89 gridlines are in the solar cell.) The value that is determined from the formula is the base finger spacing. From there the finger spacing for the next fourteen spaces is calculated and recorded by taking the multiple of the base finger spacing (all the fingers are of the same width.) Then the four-point probe system was used to run the current through the contacts (present at the metal/semiconductor interface) of the solar cell. The probes were placed on the solar cell and positive 20 μA of current was run through the fingers of the solar cell and the resulting voltage was recorded. This process is repeated using negative 20 μA . The resulting voltages was measured with 2401 Keithley Source Meter. The initial voltage reading was around 2 mV and generally increases at a constant rate.

From there on, one probe was left on the same finger, while the other probe was moved from finger to finger to stimulate increasing transfer length. This process was repeated and the data was collected and represented in an excel spreadsheet as shown below in Figure 4.2. Before the data was recorded in the spreadsheet the solar cell width must be entered as 2 mm. The excel spreadsheet calculates the results based on the input data and displays the progression of values using a real-time graph. The calculated data portion (sheet resistance and contact resistance) was collected and stored in a separate excel spreadsheet for further analysis.

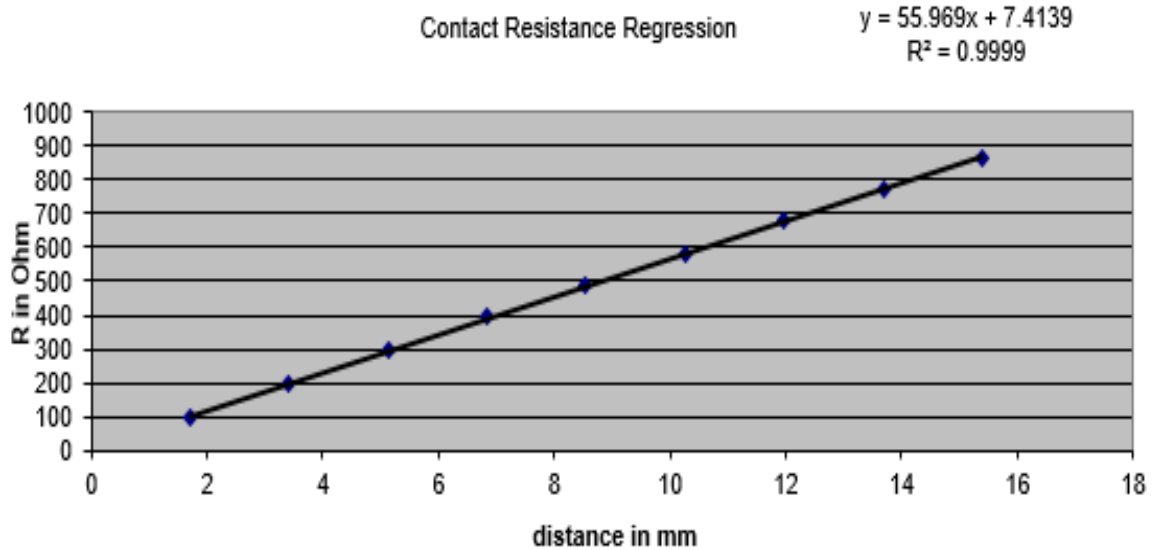


Figure 4.2: Typical graph for calculating the contact resistance with R^2 value.

An important assumption made in this approach of measuring the contact resistance is that the resistivity of the metal is much lower than the contact resistance [33]. With that assumption, the formula used in the spreadsheet to calculate the total resistance (R_T) reduces to

$$R_T = \frac{R_s}{W}L + 2R_c \quad (12)$$

where R_s , L , W and R_c are emitter sheet resistance, length of gridline, width of gridline and contact resistance, respectively. In the limit of a zero-length resistor, the residual resistance would be just twice the contact resistance. This can be found from the graph by extrapolating back to $L = 0$. Figure 7 shows a typical graph used in the spreadsheet for calculating the contact resistance.

Table 4.2: Contact resistance measurement result for the cell with tellurium and without tellurium containing paste

Cell	R(contact) mΩ-cm ²	R(sheet) Ω/sq.	FF (%)	R(series) mΩ-cm ²
TeO ₂ -1	4.02	91	79.4	0.6568
HP-1	5.41	100	79.5	0.8373
Non-TeO ₂ -1	12.6	90	68.8	2.8416

Table 4.2 shows the analysis of the contact resistance of TeO₂ containing paste and the one without TeO₂. All the pastes have micro Ag particles. The paste which contains TeO₂ shows a lower contact resistance compared to the two pastes, the commercial and non-TeO₂ containing. The lower contact resistance results from the action of TeO₂, which decreases the viscosity of the molten glass during contact firing and enable the glass to etch the ARC uniformly. This uniform etching produces larger contact area than the counterpart pastes and forms more sliver crystallites underneath the metal contacts, which helps in the current collection.

4.3 Scanning Electron Microscopy:

The scanning electron microscope is often the preferred starting tool for analytical microscopy because of its versatility and the wide range of information it can provide [34]. In scanning electron microscopy (SEM), a focused beam of high-energy electrons is scanned over the surface of a material. The electron beam interacts with the material, causing a variety of signals—secondary electrons, back-scattered electrons, X-rays, and photons-- each of which may be used to characterize a material with respect to specific

properties. State-of-the-art SEMs provide remarkable analytical versatility and a wide magnification range from 20x to 650,000x. In this study, a part of the 150 E-beam Lithography System, which has a maximum amplification of 1,000,000X, was used. The SEM generates electrons and accelerates them in an energy range of 0.1-30 keV. For the SEM used in this work, the electron beam spot size was 20 nm while the accelerating voltage was 10-15KeV.

Backscattered electrons (BSE) are electrons that escaped the sample and are useful for compositional contrast in the specimen. Secondary electrons are collected from all surfaces that the beam strikes. This results in a high collection efficiency of secondary electrons from most surfaces, even partial collection from surfaces tilted away from the detector. Thus, secondary electrons are a tool for a topographical analysis of the specimen surface. SEM was then performed at the gridline/Si interface.

Figure 4.3 shows the SEM micrograph for the TeO₂ containing paste. Figure 4.4 shows the SEM micrograph for the non-containing TeO₂ paste. Figure 4.5 displays the SEM micrograph of the commercial paste. The microstructure of the interfacial contact region of screen-printed c-Si solar cells is complex and non-uniform, with regions of both ultra-thin (electrically functional) and thick (electrically non-functional) glass layers [35] as in Figures 4.3, 4.4 and 4.5. The glass layer is formed due to the reaction of the Ag paste and ARC. The difference in the Ag crystallite size at the interface of silicon and gridline is observed.

During firing, the sintering of the Ag grain causes the dimensional changes at the interface. This dimensional change causes the variation of the thickness of the glass layer.

From the SEM images, we can see that using TeO_2 containing paste, an ultra-thin glass layer is present at the interface which acts as a low resistance path for electron tunneling and this results in a decrease of contact resistance.

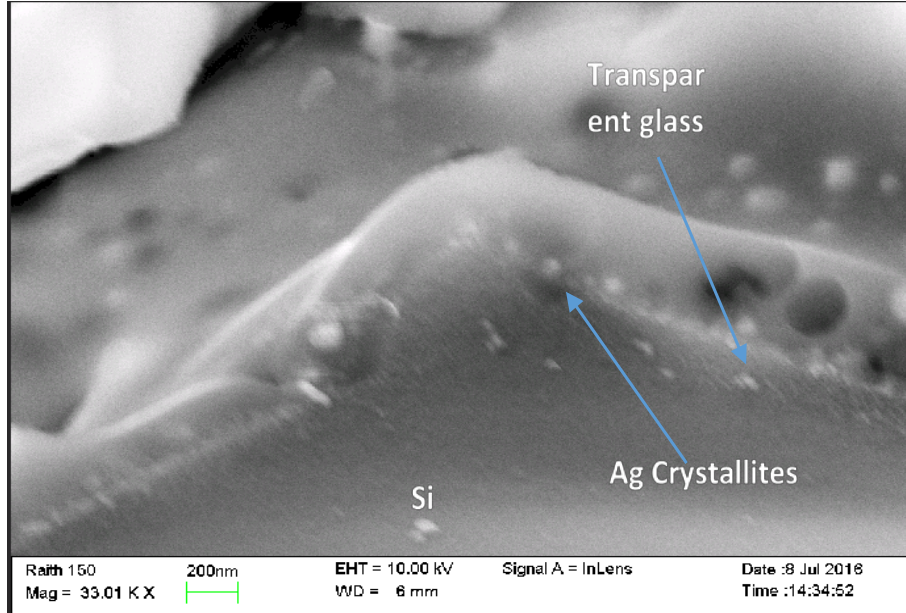


Figure 4.3: Cross sectional SEM image of the interface of Ag contact and Si emitter with TeO_2 containing paste

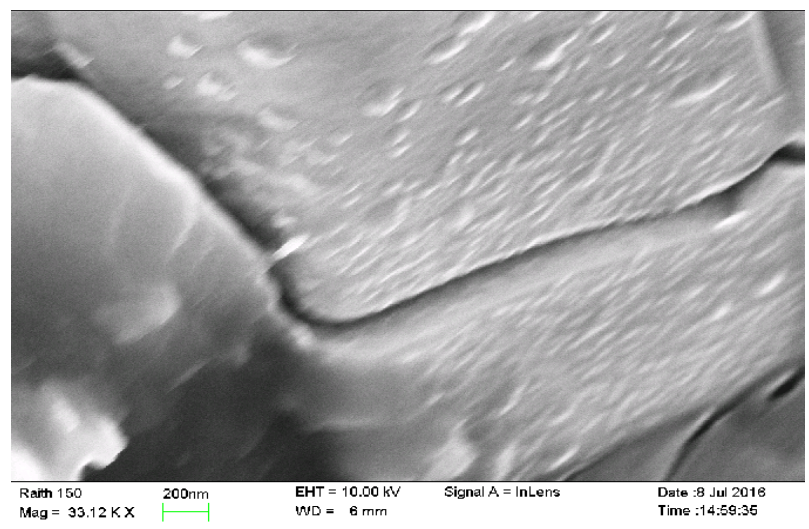


Figure 4.4: Cross sectional SEM image of the interface of Ag contact and Si emitter non- TeO_2 containing paste

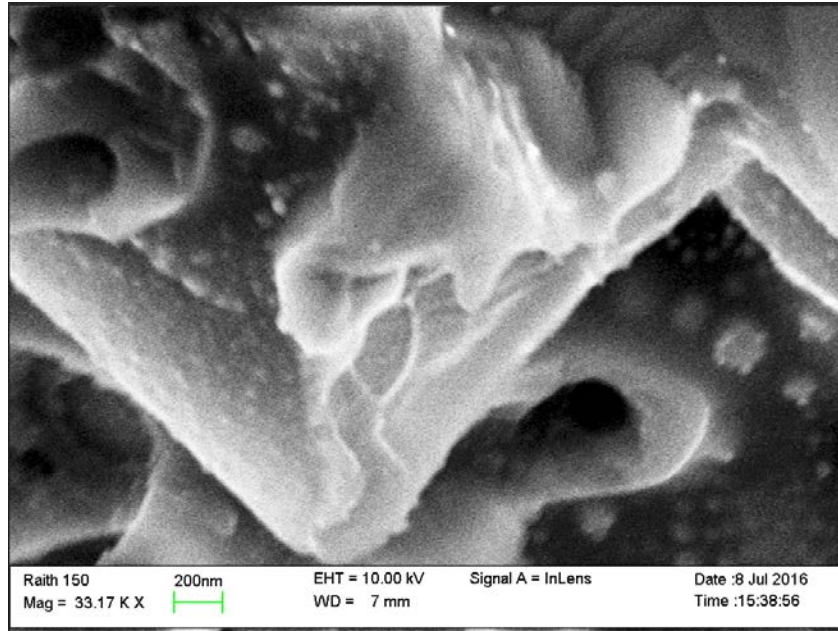


Figure 4.5 Cross sectional SEM image of the interface of Ag contact and Si emitter of commercial paste

4.4 Energy Dispersive Spectrometry (EDS)

The operation of the energy dispersive spectrometer (EDS) involves the absorption of an X-ray photon, which leads to the ejection of a photoelectron [32]. Thus, electron hole pairs are generated. Holes and electrons are separated by the electric field because of the applied reverse bias voltage and are collected at the p and n electrodes, respectively. This results in a charge pulse that is converted into a voltage by a charge-to-voltage converter circuit (also called a preamplifier) that makes use of a capacitor for charging and discharging as well as a field effect transistor (FET) to convert the charge into voltage. In this study, we are using a JEOL SEM with a resolution of 3nm, acceleration voltage is from 0.3Kv to 30Kv.

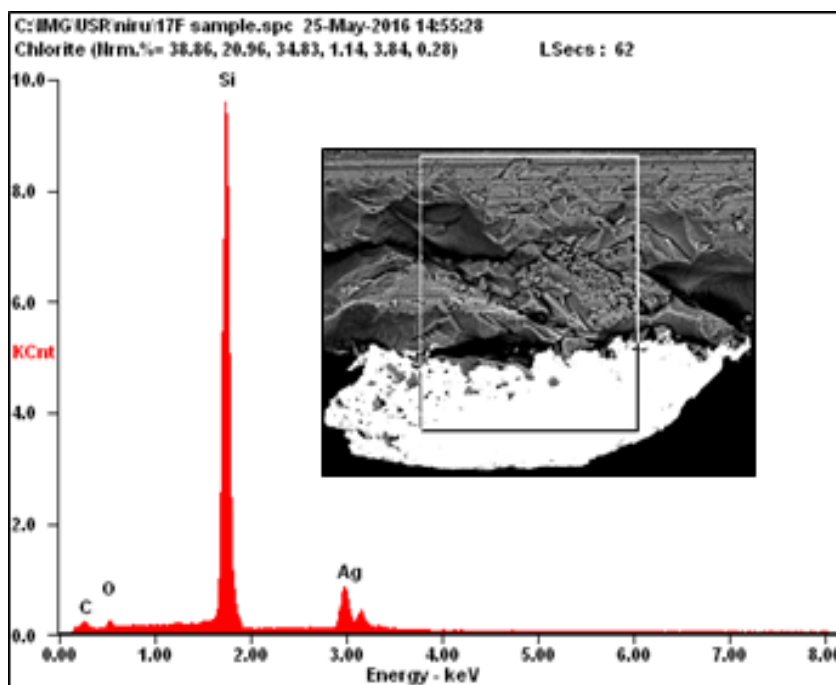


Figure 4.6: EDS analysis of the cell with paste TeO₂

EDS of the gridline for the three pastes are shown in Figures 4.6 to 4.8, respectively. From where a portion is used to assess the elements contents after contact firing. It is observed that there is no presence of tellurium at the interface or in the gridlines. This is quite good because of the environmental issues. Thus, either the TeO₂ is a catalyst that or it is below the detection limit of EDS.

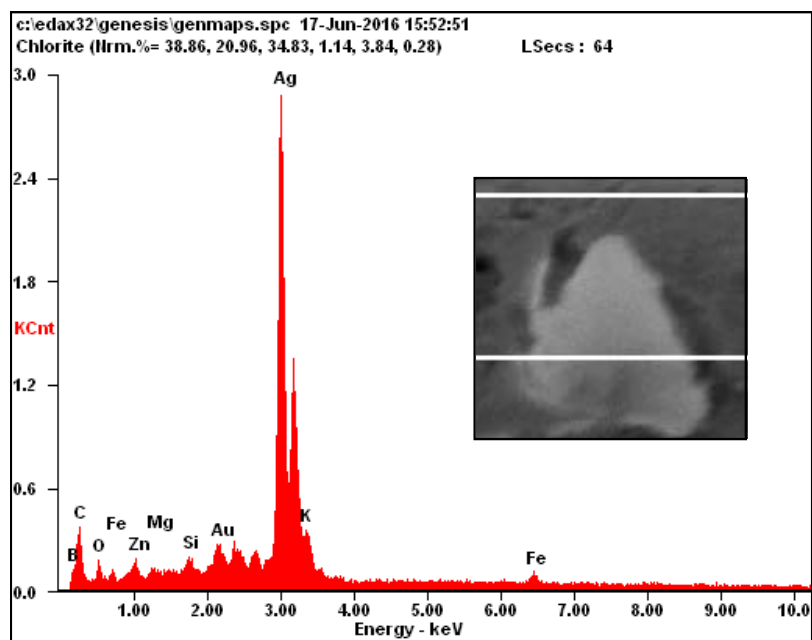


Figure 4.7: EDS analysis of the cell with non TeO₂ containing paste

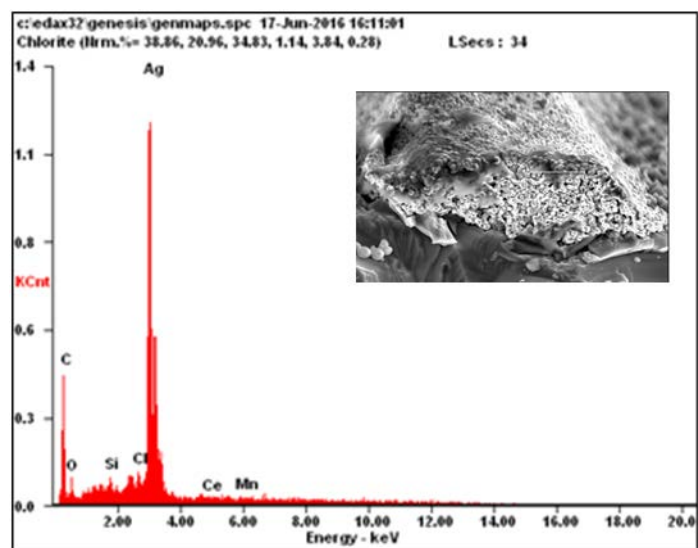


Figure 4.8 EDS analysis of the cell with commercial paste

4.5 Conclusion

The primary aim of this work was to understand the effect of TeO_2 on the series resistance of a homogeneous high sheet resistance emitter (90-100 Ω/sq) solar cell. By adding TeO_2 to the front Ag paste, the contact resistance is lower than those without the additive. The series resistance in turn is lower, leading to high FF and overall efficiency. The gridline resistance is also lower (not included in the thesis) because of the TeO_2 ability to lower the molten glass viscosity during sintering and hence form a lower porous gridline than the counterpart pastes. Thus, the gridlines with TeO_2 is more conductive than the counterparts. The SEM micrographs for the three pastes show more Ag crystallites at the interface of silicon and gridline for the TeO_2 containing paste than the others. It is very satisfying to note that the Te or its oxide is not detected after contact firing. Therefore, TeO_2 can be considered a catalyst to enhance ohmic contact formation on high sheet resistance emitter. However, it may also be that the concentration of the Te or its oxide may be too low to be detected by EDS.

REFERENCES

- [1] H. Park, J. S. Lee, S. Kwon, S. Yoon and D. Kim, *Curr. Appl. Phys.*, 10, 113118
- [2] M. Hilali, S. Sridharan, C. Khadilkar, et al., *J. Electron. Mater.* 35 (2006) 2041–2047.
- [3] Veysel Unsur “Understanding the solar cell contact formation by digital inkjet printing technique” Thesis report 2013- University of North Carolina at Charlotte..
- [4] Abasifreke Ebong and Nian Chen “Metallization of crystalline silicon solar cells: A review” HONET 9th conference December 2012.
- [5] Dr. Weiming Zhang. “How Silver Paste Can Improve Silicon Solar Cell Performance/Cast Ratio” Technical report 2006.
- [6] Mohamed M. Hilali “Understanding and development of manufacturable screen printed contacts on high sheet-resistance emitters for low-cost silicon solar cells” – Thesis- Georgia Institute of Technology, August 2005.
- [7] pveducation.org/pvcdrom/design/solar-cell-design-principles
- [8] Barbara Swatowska, Tomasz Stapinski, Kazimierz Drabczyk , Piotr Panek “The role of antireflective coatings in silicon solar cells – the influence on their electrical parameters” *Optical Application*, Vol. XLI, No. 2, 2011.

- [9] Khuram Ali, Sohail A. Khan, M. Z. Mat Jafri “Effect of Double Layer (SiO₂/TiO₂) Anti-reflective Coating on Silicon Solar Cells” Int. J. Electrochem. Sci., 9 (2014) 7865 – 7874.
- [10] Christopher Petti, Bonna Newman, Robert Brainard, Jian Li “Optimal thickness for crystalline silicon solar cells”- technical report
- [11] Y. Komatsu et al., “Sophistication of doping profile manipulation – emitter performance improvement without additional process step”, in 23th EUPVSEC (Valencia, Spain, 2008) p. 1924.
- [12] Ferdiansjah and Faridah “Effect of bulk doping level and wafer thickness on the performance of monocrystalline silicon solar cell” ARPN Journal of Engineering and Applied Sciences, 2016.
- [13] Vineet Kumar Singh, Jampana Nagaraju “Effect of diffusion parameters on the efficiency of c-Si solar cell” Adv. Mater. Lett. 2015, 6(7), 600-606
- [14] pveducation.org/pvcdrom/design/metal-grid-pattern.
- [15] Gunnar Schubert “Thick Film Metallization of Crystalline Silicon Solar Cells Mechanisms, Models and Applications” Thesis dissertation in August 2006- an der Universität Konstanz.

- [16] D. L. Meier, E. A. Good, R. A. Garcia, B. L. Bingham, S. Yamanaka, V. Chandrasekaran and C. Bucher “Determining components of series resistance from measurements on a finished cell” 2006 IEEE.
- [17] Ali Cheknanea, B. Benyoucefa, J.-P. Charlesb, R. Zerdoumc, M. Trarid. “Minimization of the effect of the collecting grid in a solar cell based silicon” Elsevier B.V. July 2004.
- [18] A. Ebong, V. Upadhyaya, B. Rounsaville, D. S. Kim, K. Tate and A. Rohatgi “18% large area screen-printed solar cells on textured mcz silicon with high sheet resistance emitter” IEEE Photovoltaic Specialists Conference 2:1326 - 1329 · June 2006
- [19] A. Ebong “Overcoming the technological challenges of contacting homogeneous high sheet resistance emitters (HHSE)” 26th European Photovoltaic Solar Energy Conference and Exhibition.
- [20] A. Ebong and A. Rohatgi “Investigation of new screen-printed pastes from heraeus incorporated for high efficiency silicon solar cells” Final Technical report, 2006
- [21] S. Körner ,a, F. Kieferb, R. Peibstb, F. Heinemeyerb, J. Krügenerc, M. Ebersteina “Basic study on the influence of glass composition and aluminum content on the Ag/Al paste contact formation to boron emitters” 5th Workshop on Metallization for Crystalline Silicon Solar Cells doi:10.1016/j.egypro.2015.03.284

- [22] M. M. Hilali, A. Rohatgi, and S. Asher, IEEE Trans. on Elect. Dev., 51, 948-955 (2004)
- [23] G. C. Cheek, R. P. Mertens, R. V. Overstraeten and L. Frisson, “Thick-film metallization for solar cell applications”, IEEE Trans., on Electron Dev., Vol. ED-31, no. 5, 1984. M. M. Hilali, A. Rohatgi, and S. Asher, IEEE Trans. on Elect. Dev., 51, 948-955 (2004)
- [24] Nakamura, Naoto Shindo, Tadashi Kanasaku, “Conductive paste for forming a Solar cell electrode” US 2011/0095240 A1 Masami Apr. 28, 2011
- [25] Shizuharu Watanabe, Takayuki Koderu, Takashi Ogihara “Preparation and sintering of tellurium-doped silver powder for electrodes in silicon solar cells” Journal of the Ceramic Society of Japan · May 2015
- [26] K. Batchu, V. Unsur and A. Ebong, (2015), “The impact of Ag particle size and rapid thermal processing belt speed on contact resistance of a silicon solar cell”, in Proceedings, 12th HONET conference, Islamabad – Pakistan, pp. 43-46.
- [27] K. Firor, S. J. Hogan, J. M. Barrett, and R. T. Coyle, “Series Resistance Associated with Thick-Film Contacts to Solar Cells” Proceedings of the 16th IEEE Photovoltaic Specialists Conference, 1982, pp. 824-827.
- [28] Gunnar Schubert “Thick Film Metallization of Crystalline Silicon Solar Cells Mechanisms, Models and Applications” Thesis dissertation in 2006

- [29] Ali Cheknanea, B. Benyoucefa, J.-P. Charlesb, R. Zerdoumc, M. Trarid.
“Minimization of the effect of the collecting grid in a solar cell based silicon
- [30] Kenneth Warren Hang, Brian J. Laughlin, Kurt Richard Mikeska, Carmine Torardi,
Paul Douglas V “Thick-film pastes containing lead and Tellurium-oxides, and their use in
the manufacture of semiconductor devices” Alan Frederick Carroll, US 8,497,420 B2- June
2013
- [31] Zeghbroeck, V. (2002), 3.5.4 Contact Resistance to a thin semiconductor layer,
Colorado ecee, (N/A), 1-8
- [32] Meier, Daniel, Schroder, Dieter. (1984) Contact Resistance in a Solar Cell - A Review,
IEEE Xplore, (ED-31), 637-646
- [33] Bock, M. E., (2004), Low-level Resistance Characterization, AMP Journal of
Technology, (3). 64-68
- [34] D. K. Schroder, Semiconductor Material and Device Characterization, New York:
John Wiley & Sons, Inc., 1990.
- [35] “Sintering behavior of silver conductive thick film with frit in information display”
Seongjin Hwang & Sangwook Lee & Hyungsun KimJ, Electroceram (2009) 23:351–355